CHINA FOUNDRY Research & Development
Vol. 21 No. 3 May 2024
www.springer.com/41230
https://doi.org/10.1007/s41230-024-4009-6

Thermal fatigue and wear of compacted graphite iron brake discs with various thermomechanical properties

***Gui-quan Wang[1], Zhuo Xu[1], Zhong-li Liu[1], Xiang Chen[2, 3], and Yan-xiang Li[2, 3]**

1. School of Nuclear Equipment and Nuclear Engineering, Yantai University, Yantai 264005, Shandong, China

2. School of Materials Science and Engineering, Tsinghua University, Beijing 100084, China

3. Key Laboratory for Advanced Materials Processing Technology, Ministry of Education, Beijing 100084, China

Abstract: The increase in payload capacity of trucks has heightened the demand for cost-effective yet high performance brake discs. In this work, the thermal fatigue and wear of compacted graphite iron brake discs were investigated, aiming to provide an experimental foundation for achieving a balance between their thermal and mechanical properties. Compacted graphite iron brake discs with different tensile strengths, macrohardnesses, specific heat capacities and thermal diffusion coefficients were produced by changing the proportion and strength of ferrite. The peak temperature, pressure load and friction coefficient of compacted graphite iron brake discs were analyzed through inertia friction tests. The morphology of thermal cracks and 3D profiles of the worn surfaces were also discussed. It is found that the thermal fatigue of compacted graphite iron discs is determined by their thermal properties. A compacted graphite iron with the highest specific heat capacity and thermal diffusion coefficient exhibits optimal thermal fatigue resistance. Oxidization of the matrix at low temperatures significantly weakens the function of alloy strengthening in hindering the propagation of thermal cracks. Despite the reduced hardness, increasing the ferrite proportion can mitigate wear loss resulting from low disc temperatures and the absence of abrasive wear.

Keywords: compacted graphite iron; brake disc; thermomechanical properties; thermal fatigue; wear

CLC numbers: TG143.5 **Document code:** A **Article ID:** 1672-6421(2024)03-248-09

1 Introduction

During a braking process, the kinetic and potential energy of the vehicle are converted into heat at the friction surface of the discs by heat generation [1, 2]. Most heat is absorbed by brake pads and discs, causing the temperature to increase and distribute in a nonuniform manner [3]. As trucks continue to develop toward higher payload capacity, brake discs undergo more severe thermal-mechanical stress and wear resulting from the frequent acceleration-deceleration processes and hard braking events [4-6].

Critical service performances of brake discs involve resistance to thermal fatigue cracking, stability in friction coefficient and durability against wear. These performances simultaneously demand excellent thermal and mechanical properties from disc materials. Increasing the tensile strength and hardness is beneficial for improving resistance against cracking and wear [7, 8]. A high specific heat capacity and a high thermal diffusion coefficient are beneficial for reducing the friction fade, thermal stress and wear by decreasing the disc temperature and unifying the temperature distribution [9-12].

Compacted graphite iron (CGI) is considered as the preferred material for brake discs of trucks and rally cars due to its superior thermal stability and fewer oxidation paths at elevated temperatures [13-15]. However, low heat transfer capacity limits the improvement of service performance in CGI brake discs. Increasing the vermicularity can improve heat diffusion by providing additional pathways for heat transfer. But this process significantly decreases the tensile strength caused by the decreased amount of

***Gui-quan Wang**

Male, born in 1985, Ph. D. His research interests mainly focus on the cast alloying materials.

E-mail: wgq19@ytu.edu.cn

Received: 2024-01-07; Accepted: 2024-03-29

spherical graphite [16, 17]. The ratio of ferrite to pearlite is also an important microstructural characteristic [16, 18]. A high proportion of ferrite can increase the heat transfer capacity of the matrix because ferrite exhibits better thermal conductivity than that of pearlite [16]. Nevertheless, soft ferrite decreases strength and hardness. Adding alloying elements can reinforce ferrite and thus improve its strength and hardness [19]. In addition, alloying additions strongly reduce the thermal diffusion capacity of the matrix for the scattering of soluted atoms [20]. A high-performance CGI brake disc requires a balance between thermal and mechanical properties. Since maintaining a high and stable level of vermicularity is difficult and costly in practical production, controlling the matrix characteristics is a feasible method to improve the performances of CGI discs. However, limited studies have simultaneously investigated the thermal fatigue and wear behaviors of CGI brake discs with various thermomechanical properties.

To establish an experimental foundation for improving the performance of CGI brake discs, their thermal fatigue resistance and wear tests were conducted. Three CGI brake discs with various thermal and mechanical properties were produced by adjusting the proportion and strength of the ferrite. The temperature change, pressure load and friction coefficient were measured throughout the braking process. The thermal fatigue cracking and wear behaviors were subsequently discussed based on SEM observations and 3D profiles.

2 Materials and experiment

2.1 Materials

Three groups of CGI ventilated discs were produced by a 250 kg medium-frequency induction furnace. Steel scrap, pig iron, ferromolybdenum, ferro-silicon, copper, tin and carburizer were used as charge materials. The mixture was heated to 1,520 °C and held for approximately 10 min and subsequently transferred to a ladle. The sandwich vermicularizing method was used with FeSiMgCe (0.38%) and FeSiBa (0.4%) at the bottom of the ladle. Three brake disc castings were poured at 1,420 °C for each composition. The chemical compositions of the brake discs are listed in Table 1. Alloying elements with large atomic radii, Sn and Mo, were used to reinforce the matrix. Moreover, Sn could also strongly change the ferrite/pearlite ratio.

Table 1: Chemical composition of CGI brake discs (wt.%)

Discs	C	Si	Mn	P	S	Mo	Cu	Sn	Mg	Fe
BV-1	3.60	2.38	0.45	0.039	0.027	0.35	0.59	0.036	0.019	Bal.
BV-2	3.56	2.42	0.45	0.042	0.026	0.35	0.60	0.046	0.020	Bal.
BV-3	3.59	2.46	0.46	0.043	0.021	0.45	0.60	0.025	0.021	Bal.

2.2 Microstructural characterization

For each composition, one disc was cut to prepare the samples. Subsequently, the microstructure and properties were observed and measured. Metallographic samples (Φ10 mm×10 mm) were used to estimate the graphite content and vermicularity based on ISO 16112:2017. The metallographic samples were then etched using 4% nital for 8 s to reveal the ferrite and pearlite. The proportion of ferrite was calculated by the ratio of ferrite to pearlite using quantitative metallography with Image Pro software. The microhardness of the ferrite was measured by an automatic Qness Q60+ microhardness tester under a 500 g load for 10 s. All the microstructure characteristics were the average values taken from eight fields.

2.3 Thermal and mechanical properties

The thermal diffusion coefficients and specific heat capacities at different temperatures were measured between 25 °C and 500 °C by a NETZSCH LFA 457HT laser flash instrument and a NETZSCH STA 449F3 differential scanning calorimeter, respectively. The average thermal expansion coefficient was measured by a Hengjiu HPY-1 thermal dilatometer at a heating rate of 10 °C·min^{-1} from 25 °C to 500 °C. Tensile strength was measured via tensile tests using dog-bone test bars (5 mm in gauge diameter and 30 mm in gauge length). The Brinell hardness was determined by an HB-3000 hardness tester on the samples cut from tensile test bars.

2.4 Inertia friction test

A LINK 3000 inertia friction test bench was used to investigate the thermal fatigue and wear of CGI discs according to the ECE R90 r3. The same type of brake pads composed of resin, fibers, and wear-resistant alloy was used for all tests. The test parameters are listed in Table 2. All the discs were burnished according to the bedding-in procedure at first to ensure that the thermal fatigue test conditions were consistent. The discs were subsequently tested according to the thermal fatigue procedure. In this procedure, the initial and peak temperatures were recorded, while the mean coefficients of friction were calculated according to the average output torque and input pressure. The configurations of the tester and the location of the thermocouple are shown in Fig. 1. The dimensions of the CGI disc used in this work are shown in Fig. 2. The test procedures are summarized as follows:

(1) Bedding-in procedure

One hundred brake applications were carried out from 60 km·h^{-1} to 30 km·h^{-1}, with deceleration alternating between 1 m·s^{-2} and 2 m·s^{-2}. The initial temperature of the disc started at room temperature. After 30 applications, the initial temperature

of the disc was decreased to 300 °C using cooling air at 28 °C. The speed of the cooling air was maintained at 19.3 km·h^{-1}.

Table 2: Parameters used in the inertia friction test

Item	Details
Test parameters	Test type: front axle brake disc
	Maximum mass of vehicle: 2,110 kg
	Dynamic rolling radius: 0.316 m
	Rotary inertia: 81.1 kg·m^2
	Piston diameter×number: 60 mm×1
	Effective radius of disc: 134.75 mm

(2) Thermal fatigue procedure

In total, 150 braking cycles were applied. Each cycle included 2 brake applications. In the first application, the disc was braked from 180 km·h^{-1} to 20 km·h^{-1}. Subsequently, the disc was cooled for 70 s using cooling air at 28 °C. The second application was a repetition of the first one, once again braking from 180 km·h^{-1} to 20 km·h^{-1}. Following this, the disc was cooled until its temperature reached 100 °C, which then became the initial temperature for the next cycle. The deceleration throughout the process was maintained at 5 m·s^{-2}, and the cooling air speed was set at 53.1 km·h^{-1}.

The discs subjected to the inertia friction test were then cut for observation. The worn surfaces were observed by an optical microscope and a JEOL field-emission scanning electron microscope (SEM). The microscopic 3D profiles of the worn surfaces were measured by a ZYGO optical 3D profilometer.

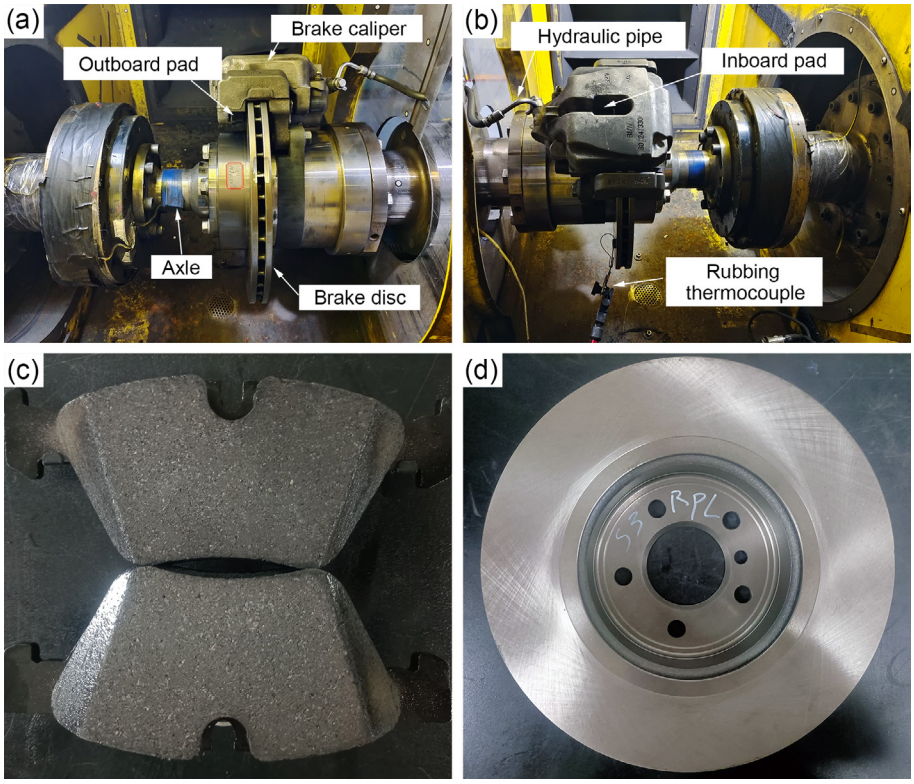

Fig. 1: Configurations of inertia friction test (a and b), brake pads (c), and brake disc before the test (d)

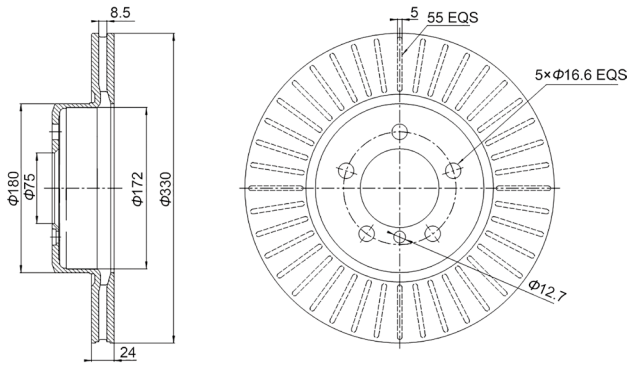

Fig. 2: Dimensions of the CGI disc (unit: mm)

3 Results and discussion

3.1 Microstructures and properties

Typical microstructures of the three CGI discs are shown in Fig. 3. The corresponding microstructural characteristics, mechanical properties and thermal expansion coefficients are summarized in Table 3. Figure 4 illustrates the changes in the thermal diffusion coefficient and specific heat capacity concerning temperature. An almost uniform graphite content and vermicularity are obtained by similar carbon equivalent and vermicularizing processes. The differences in the microstructure mainly involve the proportion and microhardness of ferrite. The BV-3 disc exhibits the highest ferrite proportion, while

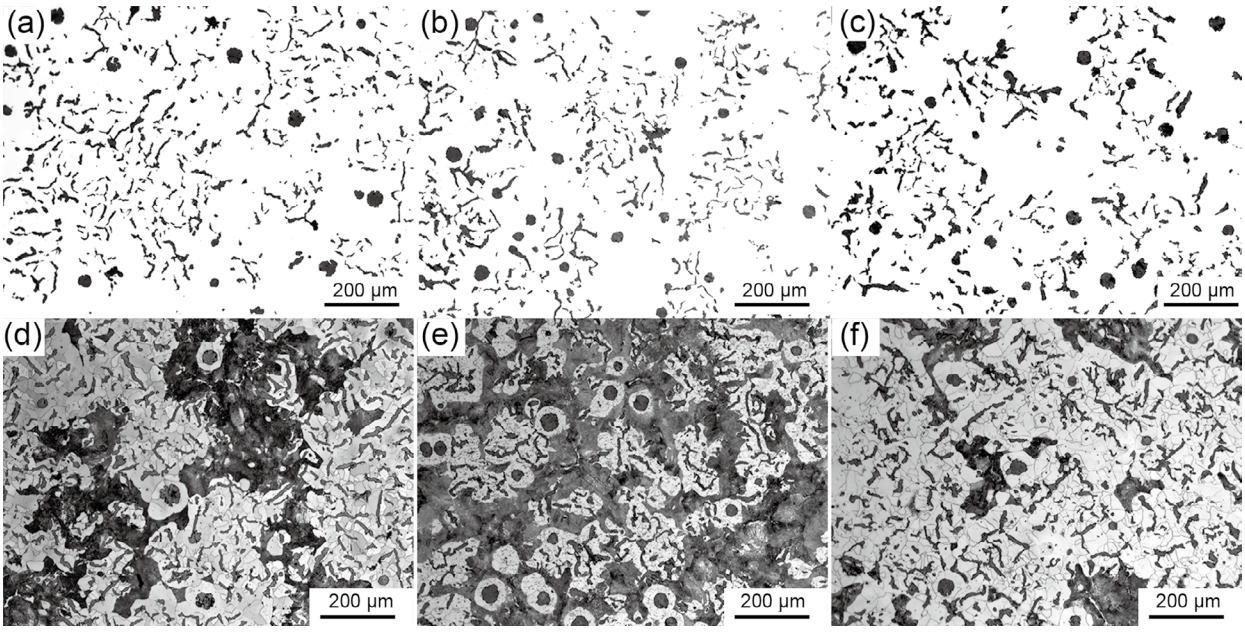

Fig. 3: Graphite morphologies of BV-1 (a), BV-2 (b) and BV-3 (c) and the matrix of BV-1 (d), BV-2 (e) and BV-3 (f)

Table 3: Microstructural characteristics and properties of CGI brake discs

Microstructural characteristics and properties	BV-1	BV-2	BV-3
Graphite percentage (%)	9.4 ± 0.3	9.7 ± 0.5	9.3 ± 0.5
Ferrite proportion (%)	62.3 ± 3.4	48.0 ± 1.4	73.6 ± 4.8
Vermicularity (%)	81.2 ± 3.3	82.4 ± 2.4	84.1 ± 4.1
Tensile strength (MPa)	406 ± 6	438 ± 8	350 ± 5
Brinell hardness (HBW)	193 ± 6	212 ± 5	177 ± 2
Microhardness of ferrite (HV)	178.0 ± 23.1	188.2 ± 17.0	177.7 ± 11.8
Thermal expansion coefficient (10^{-6}·K^{-1})	14.3	13.9	14.6

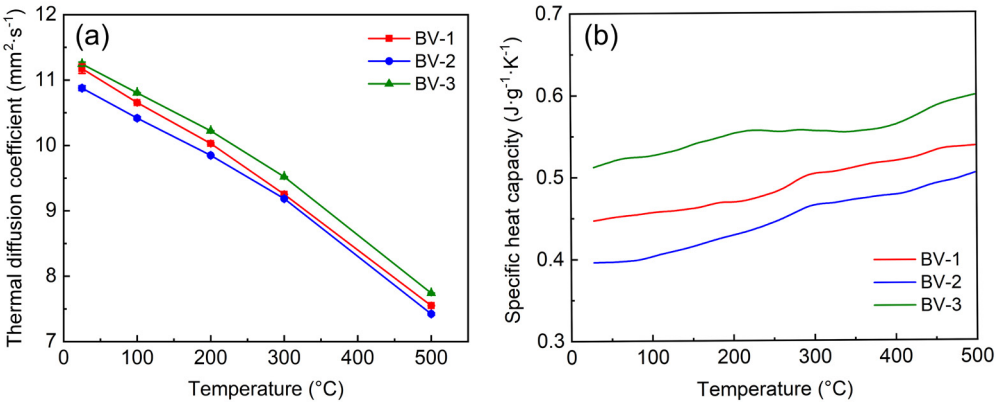

Fig. 4: Thermal diffusion coefficient (a) and specific heat capacity (b) of CGI brake discs

the BV-2 disc has the lowest ferrite proportion. This difference is attributed to their different Sn contents, as Sn significantly promotes the formation of pearlite [18]. Both the large atomic radius elements Sn and Mo can effectively strengthen the iron matrix [13]. The Sn content in the BV-2 disc is higher than that in the BV-1 disc, resulting in a higher microhardness of ferrite. On the other hand, although the Sn content in the BV-3 disc is lower than that in the BV-1 disc, the higher content of Mo elements allows it to achieve a similar microhardness of ferrite to that of the BV-1 brake disc.

Different combinations of thermal and mechanical properties are achieved in the three CGI discs. Notably, the BV-2 disc exhibits the highest tensile strength and macrohardness, although having the lowest thermal diffusion coefficient and

specific heat capacity. This characteristic is attributed to its lower ferrite proportion. Conversely, the BV-3 disc exhibits the lowest tensile strength and macrohardness but features the highest thermal properties, owing to its higher ferrite proportion. The BV-1 disc presents moderate thermal and mechanical properties. These observed relationships are indeed expected, considering the contradictory effects associated with the proportion and strength of ferrite. Interestingly, despite the different matrices, the thermal expansion coefficients of the three CGIs are found to be similar.

3.2 Corrosion property characterization

Temperature is an important parameter that significantly affects the thermal stress, friction coefficient and wear of brake discs. The maximum temperature of the brake disc occurs at its contact surfaces with brake pads by heat generation. Then, a portion of the heat causes the disc temperature to increase via thermal absorption and diffusion, while the remainder of the heat is dissipated by thermal convection, thermal radiation and material loss.

The peak temperature (T_m) during all the braking cycles was recorded by a rubbing thermocouple, and the results are depicted in Fig. 5. Figure 5(a) illustrates the peak temperature in the first application stage. Obviously, the BV-2 disc exhibits the highest peak temperature, followed by the BV-1 and the BV-3 discs in sequence. This regularity is consistent with the thermal properties shown in Fig. 4. Under a certain generated heat, the peak temperature of the discs is mainly determined by the temperature rise and dissipation, which are related to specific heat capacity and thermal diffusion coefficient. The BV-3 disc has the lowest peak temperature because it possesses the highest specific heat capacity and thermal diffusion coefficient. A similar regularity can be found in the second application, as shown in Fig. 5(b). The peak temperature of the BV-3 disc remains the lowest. In the first 70 cycles, the peak temperature of the BV-2 disc is higher than that of the BV-1 disc. Subsequently, the peak temperature of the BV-2 discs decreases to the same level as that of the BV-1 disc. A possible reason is that more severe wear occurs on the BV-1 disc at elevated temperatures, causing more losses of material and heat.

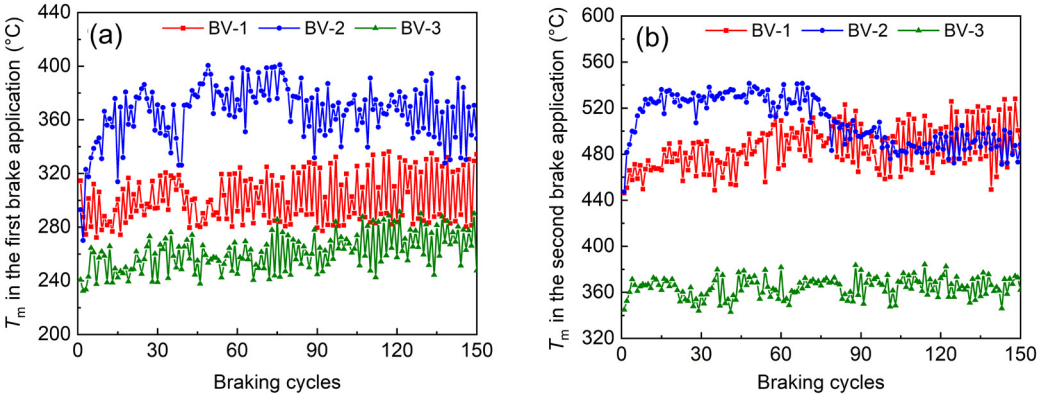

Fig. 5: Peak temperature of CGI discs in the first (a) and second (b) applications

3.3 Brake pressure and friction coefficient

Brake pressure provides a force that presses the pads against the disc, resulting in mechanical stress and friction. In each braking cycle, the brake pressure was adjusted according to the brake torque to ensure fixed deceleration. The average pressures applied from pads during the test are shown in Fig. 6.

The input pressures in the second application are lower than those in the first application for all discs. This finding implies that high temperature increases the friction force, which leads to a reduction in brake pressure. However, despite having the lowest temperature and thermal expansion, the BV-3 disc encounters the least pressure load in both the first and second brake applications.

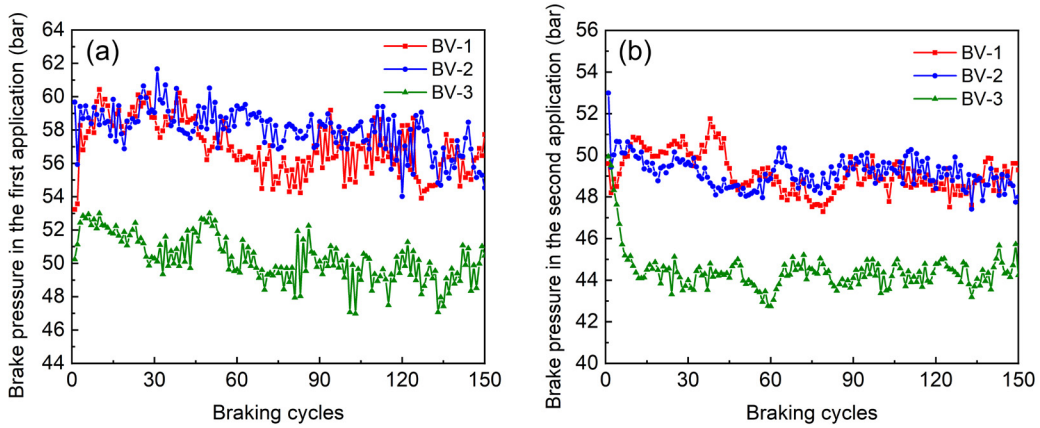

Fig. 6: Braking pressure applied to discs in the first (a) and second (b) applications

The average friction coefficients are summarized in Fig. 7. The friction coefficients show an inverse regularity to the brake pressure. In the first and second applications, the BV-3 disc, which has the lowest temperature, exhibits the highest friction coefficient. Similar values are found for BV-1 disc and BV-2 disc. All the CGI discs exhibit higher friction coefficients in the second application even through higher temperatures are produced in this stage.

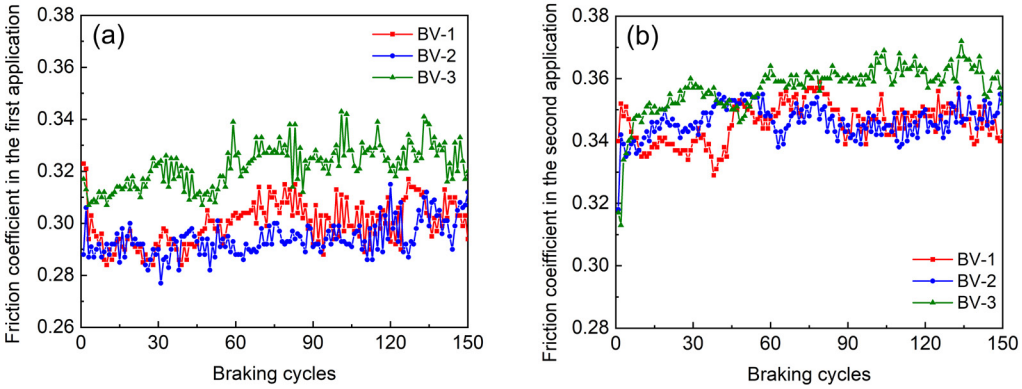

Fig. 7: Friction coefficient of CGI discs in the first (a) and second (b) applications

The variations in brake pressure and friction coefficient imply that the thermomechanical properties of discs exert complex effects on friction. High temperatures lead to a significant thermal expansion, facilitating closer contact between the discs and pads. This provides a larger friction force, resulting in a reduction in the brake pressure to maintain uniform deceleration. In addition, the low temperature of the BV-3 disc is helpful for maintaining the high mechanical properties of the disc and pads, which generates sufficient brake force to reduce the requirement of extra braking pressure.

3.4 Thermal cracks

Due to nonuniform temperature distribution and brake pressure applied from the pads, thermal cracks formed on the worn surfaces of all CGI discs, as shown in Fig. 8. Considering that cracks may be confused with scratches or covered by abrasives, the worn surface was lightly burnished. The cracks on the burnished surface are also shown in Fig. 8. No clear penetrating cracks are observed on any of the three discs. The thermal cracks appear thin and nondirectional. The long thermal cracks mainly propagate along the graphite particles. Moreover, almost all the vermicular graphite particles in Fig. 8(b) and Fig. 8(d) are connected by cracks, while fewer cracks are observed in Fig. 8(f). This finding suggests that the thermal fatigue of the BV-1 and BV-2 discs is more severe than that of the BV-3 disc.

To quantify the density of the cracks, a grid was superimposed on the burnished micrographs. The intersections between the grid and surface cracks were counted. The density of thermal cracks was defined as the number of intersections per 1 mm length. Eight fields were measured, and the average values are shown in Fig. 9. This comparison indicates that the BV-3 disc provides the best thermal fatigue resistance. This can be attributed to the low temperature and small external pressure loads during the brake cycles, as mentioned above. In other words, despite its low tensile strength, the BV-3 disc exhibits higher thermal fatigue resistance due to its high specific heat capacity and thermal diffusion coefficient.

3.5 Wear

Figure 10 displays SEM images of the worn surfaces, revealing an oxidized matrix surrounding thermal cracks across all CGI discs. This is a consequence of the tribo-oxidation process [21]. This oxidation is attributed to the decomposition and evaporation of organic components in pads, which is accelerated in the temperature range of 230–450 °C [22]. The presence of a brittle oxidized matrix weakens the role of alloy strengthening, making it less effective in resisting the propagation of thermal cracks. Moreover, this indirectly explains why discs with higher tensile strengths, such as BV-1 and BV-2, exhibit more thermal cracks. Additionally, it is noted that reducing temperature and thermal stress is a more effective approach than strengthening the matrix in mitigating thermal cracking.

As depicted in Fig. 10(b), unlike the BV-1 and BV-3 discs, the worn surface of BV-2 exhibits noticeable areas of peeling. This discrepancy may arise from more severe adhesive wear and fatigue wear in the BV-2 disc, a consequence of higher temperatures. The material loss during peeling wear contributes to the dissipation of external heat, potentially leading to a temperature decrease in the post-stage of second applications, as shown in Fig. 5(b).

Figure 11 shows the 3D profiles of the worn surfaces. Typical furrow wear can be observed on both BV-1 and BV-3 discs, while the BV-2 disc displays a distinctive combination of furrow and island-peaks. Analyzing the maximum difference (Sz) between the height and depth of the furrows reveals that the furrows on the BV-3 disc are deeper and wider compared to those on the BV-1 and BV-2 discs. This discrepancy in furrow dimensions can be attributed to the higher proportion of soft ferrite in the BV-3 disc. The furrows on the BV-2 disc contain many isolated islands randomly distributed throughout its surface. This characteristic indicates that the BV-2 disc experiences a combination of abrasive wear and furrow wear, resulting in localized erosion or stress concentration at elevated temperatures.

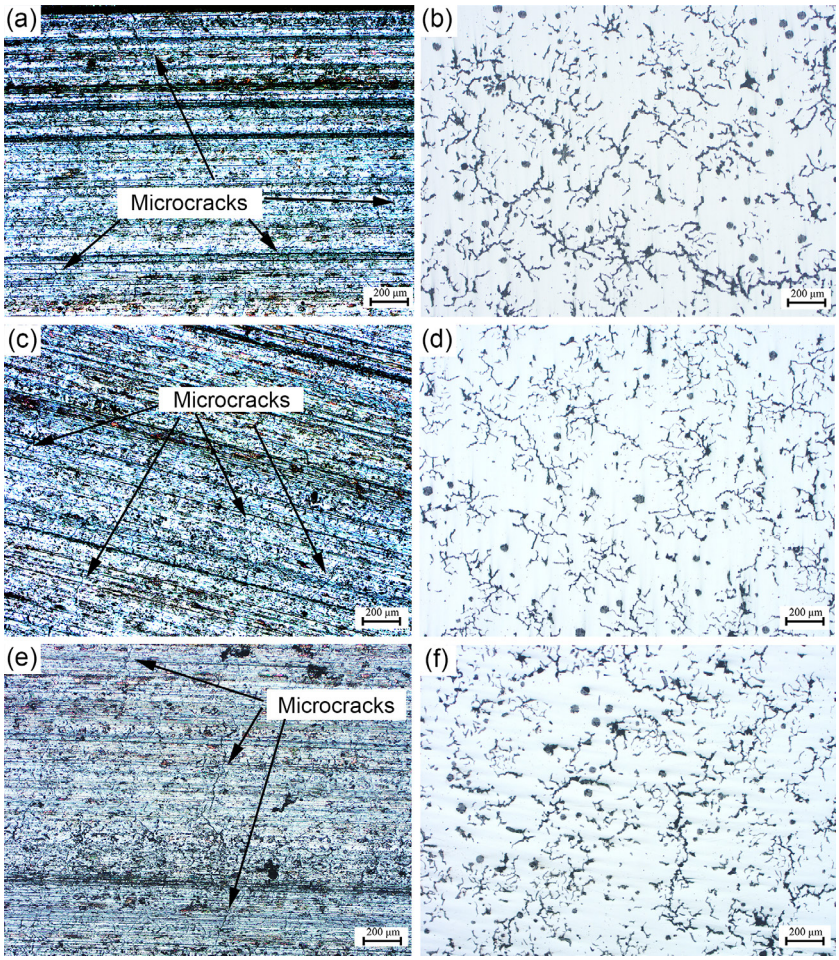

Fig. 8: Thermal cracks on the worn surfaces (a, c, e) and burnished surfaces (b, d, f): (a, b) BV-1; (c, d) BV-2; (e, f) BV-3

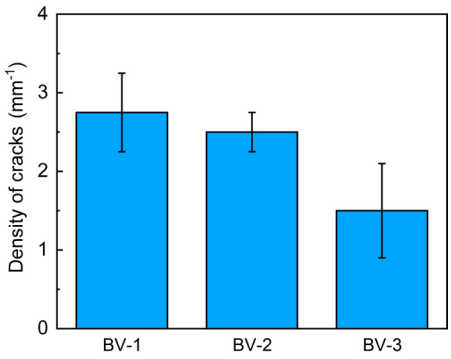

Fig. 9: Density of thermal cracks

The accumulated weight loss data are summarized in Fig. 12. Although the BV-2 disc possesses the greatest hardness, its wear is the most severe. This can be explained by the highest disc temperature and abrasive wear, resulting from the lowest specific heat capacity and thermal diffusion coefficient. Despite the deeper furrows, the wear loss of the BV-3 disc is similar to that of the BV-1 disc. This may be due to the lower temperature of the BV-3 disc maintaining its hardness at a high value. The above results indicate the complex effects of thermomechanical properties on the wear of CGI discs. A high ferrite proportion reduces the hardness of the matrix, resulting

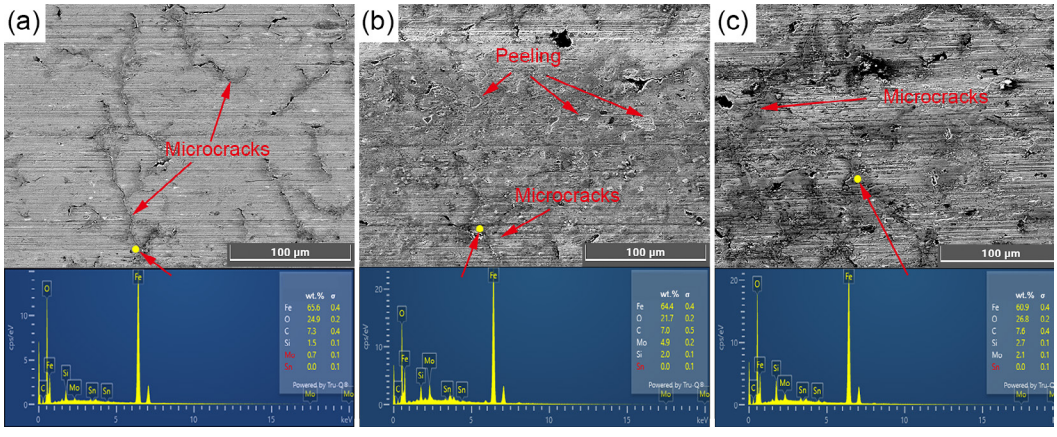

Fig. 10: Worn surfaces of CGI discs: (a) BV-1; (b) BV-2; (c) BV-3

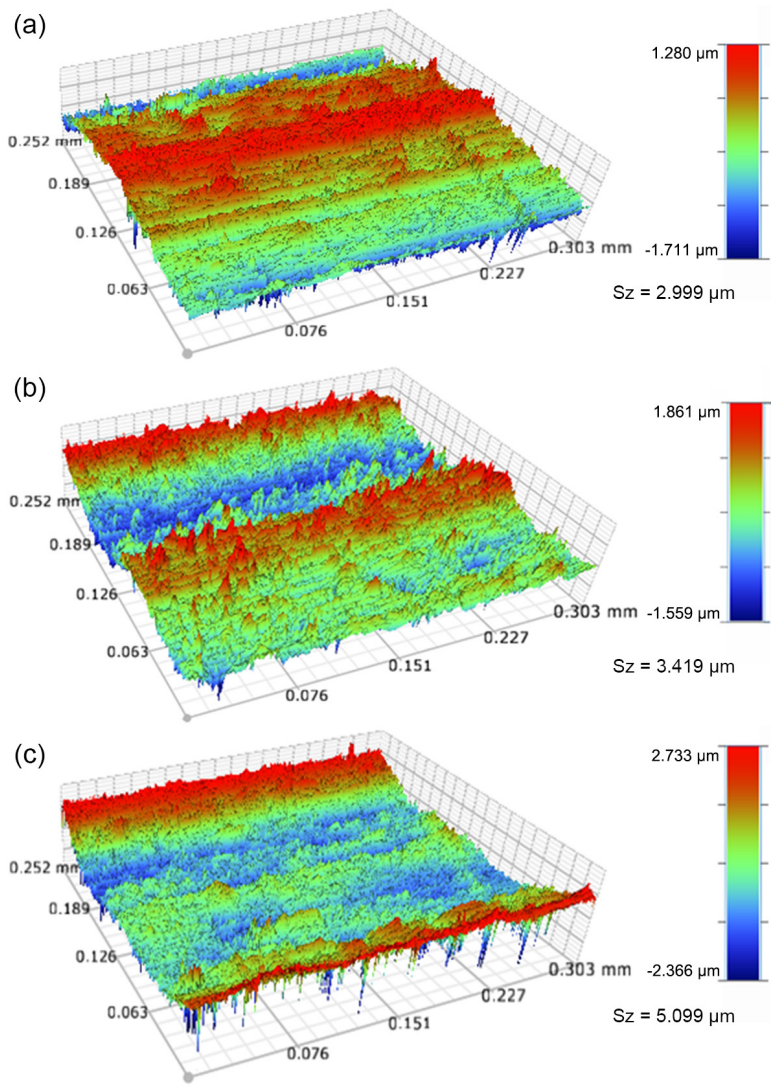

Fig. 11: Worn surfaces of the CGI discs in 3D: (a) BV-1; (b) BV-2; (c) BV-3

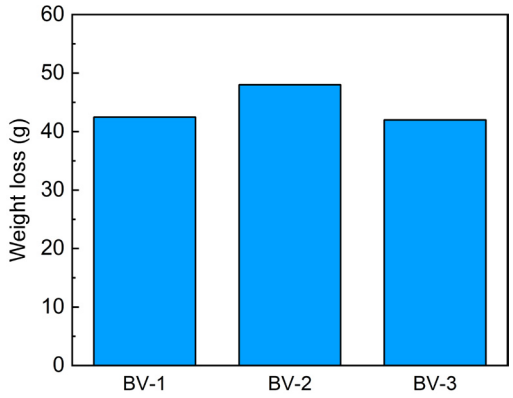

Fig. 12: Weight loss of the CGI discs

in severe furrow wear. However, the simultaneous decrease in the disc temperature helps prevent abrasive wear, contributing to the reduction in total weight loss.

4 Conclusions

The thermal fatigue and wear of CGI brake discs with various thermomechanical properties were studied via the inertia friction test. The conclusions are summarized as follows:

(1) Under identical braking inertia, a CGI disc with a higher specific heat capacity and thermal diffusivity coefficient can effectively reduce its disc temperature, leading to a decrease in the external mechanical stress imposed by the brake pads.

(2) The friction coefficient of CGI discs is intricately influenced by their structural composition and inherent properties. Higher disc temperatures increase the friction coefficient due to significant thermal expansion of both the disc and brake pads. In addition, keeping the disc temperature lower can help minimize the fade in the friction coefficient. Notably, the BV-3 disc, characterized by the highest ferrite proportion, demonstrates the peak friction coefficient owing to its superior thermal properties and the ability to sustain a lower disc temperature.

(3) The thermal fatigue of CGI discs is dominated by their thermal properties. The BV-3 disc, which exhibits the highest thermal properties, shows the fewest thermal cracks. The decomposition of pads at low temperatures facilitates the oxidation of the matrix, which accelerates the propagation of cracks. This weakens the role of alloy strengthening in resisting the expansion of thermal fatigue cracks.

(4) The wear of CGI discs is influenced by the complex interplay of their thermomechanical properties. Increasing the hardness of CGI discs through alloy strengthening does not necessarily imply an improvement in wear resistance. Such efforts may lead to more severe weight loss due to abrasive wear, a consequence of lower thermal properties and higher disc temperature.

Acknowledgment

This work was supported by the Science and Technology Innovation Development Project of Yantai (No. 2023ZDX016).

Conflict of interest

Zhong-li Liu and Yan-xiang Li are the EBMs of *CHINA FOUNDRY*. They were not involved in the peer-review or handling of the manuscript. The authors have no other competing interests to disclose.

References

[1] Pevec M, Potrc I, Bombek G, et al. Prediction of the cooling factors of a vehicle brake disc and its influence on the results of a thermal numerical simulation. International Journal of Automotive Technology, 2012, 13: 725–733.
[2] Limpert R. Brake design and safety. 3rd. ed. Warrendale: SAE International, 2011: 74–78.
[3] Belhocine A, Bouchetara M. Thermal analysis of a solid brake disc. Applied Thermal Engineering, 2012, 32: 59–67.
[4] Chen A, Kienhöfer F. The failure prediction of a brake disc due to nonthermal or mechanical stresses. Engineering Failure Analysis, 2021, 124: 105319.
[5] Wu S, Zhang S, Xu Z. Thermal crack growth-based fatigue life prediction due to braking for a high-speed railway brake disc. International Journal of Fatigue, 2016, 87: 359–369.
[6] Lu C, Shen J, Fu Q, et al. Research on radial crack propagation of railway brake disc under emergency braking conditions. Engineering Failure Analysis, 2023, 143: 106877.
[7] Li W, Yang X, Wang S, et al. Comprehensive analysis on the performance and material of automobile brake discs. Metals, 2020, 10(3): 377.
[8] Yeh C, Hwang W, Lin C. Numerical simulation on hardness distribution for a FC250 gray cast iron brake disc casting and its experimental verification. Materials Transactions, 2009, 50(11): 2584–2592.
[9] Belhocine A, Bouchetara M. Thermomechanical modelling of dry contacts in automotive disc brake. International Journal of Thermal Sciences, 2012, 60: 161–170.
[10] Maluf O, Angeloni M, Castro D, et al. Effect of alloying elements on thermal diffusivity of gray cast iron used in automotive brake disks. Journal of Materials Engineering and Performance, 2009, 18: 980–984.
[11] Liu J, Yan J, Zhao X, et al. Precipitation and evolution of nodular graphite during solidification process of ductile iron. China Foundry, 2020, 17(4): 260–271.
[12] Zhang M, Pang J, Meng L, et al. Study on thermal fatigue behaviors of two kinds of vermicular graphite cast irons. Materials Science and Engineering: A, 2021, 814: 141212.
[13] Wang G, Liu Z, Li Y, et al. Different thermal fatigue behaviors between gray cast iron and vermicular graphite cast iron. China Foundry, 2022, 19(3): 245–252.
[14] Wang X, Zhang W. Oxidation and thermal cracking behavior of compacted graphite iron under high temperature and thermal shock. Oxidation of Metals, 2017, 87: 179–188.
[15] Jing G, Sun S, Ma T, et al. Prediction of thermomechanical fatigue life in RuT450 compacted graphite cast iron cylinder heads using the Neu/Sehitoglu model. Engineering Failure Analysis, 2024, 156: 107767.
[16] Cao M, Baxevanakis P, Silberschmidt V. Effect of graphite morphology on the thermomechanical performance of compacted graphite iron. Metals, 2023, 13(3): 473.
[17] Ma Z, Tao D, Yang Z, et al. The effect of vermicularity on the thermal conductivity of vermicular graphite cast iron. Materials & Design, 2016, 93: 418–422.
[18] Selin M, König M. Regression analysis of thermal conductivity based on measurements of compacted graphite irons. Metallurgical and Materials Transactions A, 2009, 40: 3235–3244.
[19] Zeng D, Lu L, Zhang N, et al. Effect of different strengthening methods on rolling/sliding wear of ferrite-pearlite steel. Wear, 2016, 358: 62–71.
[20] Ghasemi R, Elmquist L, Svensson H, et al. Mechanical properties of solid solution-strengthened CGI. International Journal of Cast Metals Research, 2016, 29(1–2): 98–105.
[21] Verma P C, Menapace L, Bonfanti A, et al. Braking pad-disc system: Wear mechanisms and formation of wear fragments. Wear, 2015, 322–323: 251–258.
[22] Verma P C, Ciudin R, Bonfanti A, et al. Role of the friction layer in the high-temperature pin-on-disc study of a brake material. Wear, 2016, 346–347: 56–65.